Metabolic heterogeneity protects metastatic mucosal melanomas cells from ferroptosis

WEIFAN LIN[1*], XIANGWAN LU[1*], HANG YANG[1], LINXUAN HUANG[1], WUHENG HUANG[1], YULUAN TANG[1], SITUN LIU[1], HUA WANG[2] and YAN ZHANG[1]

[1]MOE Key Laboratory of Gene Function and Regulation, School of Life Sciences, Sun Yat-sen University, Guangzhou, Guangdong 510006; [2]Department of Oral and Maxillofacial Surgery, Guanghua School of Stomatology, Guanghua Hospital of Stomatology, Sun Yat-sen University, Guangzhou, Guangdong 510055, P.R. China

Abstract. Cancer heterogeneity has been proposed to be one of the main causes of metastatic dissemination and therapy failure. However, the underlying mechanisms of this phenomenon remain poorly understood. Melanoma is an aggressive malignancy with a high heterogeneity and metastatic potential. Therefore, the present study investigated the possible association between cancer heterogeneity and metastasis in melanoma. In total, two novel Chinese oral mucosal melanoma (COMM) cell lines, namely COMM-1 and COMM-2, were established for exploring methods into preventing the loss of cellular heterogeneity caused by long-term cell culture. Each cell line was grown under two different models of culture, which yielded two subtypes, one exhibited an adhesive morphology (COMM-AD), whereas the other was grown in suspension (COMM-SUS). Compared with the COMM-AD cells, the COMM-SUS cells exhibited higher metastatic capacities and autofluorescence. Further investigations indicated that the COMM-SUS cells exhibited metabolic reprogramming by taking up lactate produced by COMM-AD cells at increased levels to accumulate NADH through monocarboxylate transporter 1, whilst also increasing NADPH levels through the pentose phosphate pathway (PPP). Additionally, increased NADH and NADPH levels in the COMM-SUS cells, coupled with the upregulation of the anti-ferroptotic proteins, glutathione peroxidase 4 and ferroptosis suppressor protein 1, enabled them to resist ferroptotic cell death induced by oxidative stress during hematogenous dissemination. The inhibition of ferroptosis was found to substantially increase the metastatic capacity of COMM-AD cells. Furthermore, suppressing lactate uptake and impairing PPP activation significantly decreased the metastatic potential of the COMM-SUS cells. Thus, the present study on metabolic heterogeneity in COMM cells potentially provides a novel perspective for exploring this mechanism underlying cancer metastasis.

Introduction

Melanoma is a malignancy that has the highest rate of increase in incidence worldwide, with a high tendency for metastasis (1-3). Among other subtypes of melanoma, mucosal melanoma (MM) in the oral and maxillofacial regions is a particularly aggressive malignancy with a poor prognosis (4). A variety of treatment strategies have been utilized for improving upon the poor 5-year survival rate, such as anti-programmed death-1/programmed death-ligand-1, anti-cytotoxic T-cell lymphocyte-4 antibody immunotherapies (5,6) and oncolytic viral therapy (7,8). However, therapy for patients with MM presenting with distant metastasis remains a major challenge in the clinical setting due to the poorly understood pathological drivers.

Following metastasis, cancer cells acquire advantageous alterations in their physiology that facilitate cell proliferation, genome integrity maintenance and immune escape to survive various stresses or nutrient deprivation (9). Previous *in vivo* models have revealed that only 0.02% disseminated melanoma cells in the circulation survive to form metastases (10). This is due to the fact that disseminated cancer cells must overcome harsh environments, including physical damage from hemodynamic shear forces, immune-mediated killing, and various forms of cell death induced by genetic dysregulation, including apoptosis, anoikis and ferroptosis (11).

Ferroptosis is characterized as an reactive oxygen species (ROS)-dependent form of regulated cell death that

Correspondence to: Professor Yan Zhang, MOE Key Laboratory of Gene Function and Regulation, School of Life Sciences, Sun Yat-sen University, 135 Xingang Xi Road, Guangzhou, Guangdong 510006, P.R. China
E-mail: zhang39@mail.sysu.edu.cn

Professor Hua Wang, Department of Oral and Maxillofacial Surgery, Guanghua School of Stomatology, Guanghua Hospital of Stomatology, Sun Yat-sen University, 56 Lingyuan West Road, Guangzhou, Guangdong 510055, P.R. China
E-mail: wanghua9@mail.sysu.edu.cn

*Contributed equally

occurs downstream of iron accumulation and excessive lipid peroxidation-mediated membrane damage (12,13). Ferroptosis is initiated by polyunsaturated fatty acid peroxidation and subsequent membrane damage, of which malondialdehyde (MDA) is one of the by-products of lipid peroxidation (14-16). To date, three pathways have been demonstrated to induce ferroptosis. The glutathione peroxidase 4 (GPX4)-glutathione (GSH)-cysteine axis is the central and most upstream node of the ferroptosis death cascade (17). In addition, there are the ferroptosis suppressor protein 1 (FSP1)-ubiquinol-nicotinamide adenine dinucleotide hydrogen/NADPH (18) and the GTP cyclohydrolase I-tetrahydrobiopterin axes (19,20). Among these signaling axes, GSH is considered to be the reducing substrate of GPX4, whereby the intracellular GSH concentration is maintained by a complex homeostatic mechanism (21). Additionally, glutathione-disulfide reductase (GSR) is a glutathione reductase that catalyzes the transformation of glutathione disulfide (GSSG) to GSH. Previous studies have demonstrated that therapy-resistant cancer cells are potentially susceptible to regulation by the GPX4-/GSH-/cysteine axis, indicating vulnerability to this form of cell death (22,23). By contrast, ferroptosis-resistant cancer cells exhibit a greater viability by becoming dormant before metastasizing when favorable conditions arise (24).

During metastatic progression, cancer cells can not only remodel the tumor microenvironment to render it more suitable for secondary tumorigenesis, but also improve their potential plasticity (25). This can be mediated by metabolic reprogramming and acquisition of the ability to resist oxidative stress. Despite being generally known to be a waste product of anaerobic metabolism, lactate has been previously shown to be a major source of carbons for the tricarboxylic acid cycle (TCA) in both normal and cancerous tissues, even in the presence of glucose (26-28). Indeed, the range of lactate detected in solid tumors has been found to be 10-40 mM (29). As an indicator of metabolic reprogramming, lactate may serve as an energy source to meet the cellular energy demands and activate the associated signaling pathways (30). Monocarboxylate transporters (MCTs) are members of a cytoplasmic membrane protein family that rapidly exchange lactate to allow cells to use lactate more efficiently (31), depending on the lactate concentration and extracellular pH (28). MCTs have been reported to contribute to cancer development through multiple mechanisms, such as MCT1 and MCT4 (28,32,33). MCT1 and MCT4 are ubiquitously expressed. In addition, MCT4 has the lowest affinity for lactate among all members of MCTs and therefore primarily facilitates lactate efflux from glycolytic cells (30,34). Aerobic glycolysis has been suggested to regulate lactate production and NADH accumulation (27,35). Accumulating clinical evidence has indicated that high expression levels of MCT1 or MCT4 are associated with poorer prognosis (36-38). Furthermore, increasing MCT1 or MCT4 expression can promote colorectal, bladder, gastric, esophageal and cervical cancer cell migration and metastasis (28,33,39-42).

Cancer cell lines are extensively used to investigate caner heterogeneity; however, cancer cells tend to gradually lose heterogeneity during long-term cell culture (43-45). Therefore, in the present study, two novel MM cell lines were established to investigate whether metabolic heterogeneity can protect metastatic MM cells from ferroptosis to promote distal metastasis.

Materials and methods

Chemicals and reagents. The ferroptosis inhibitor, ferrostatin-1 (Fer-1, 10 mM, cat. no. HY-100579) and the ferroptosis inducer, Erastin (10 mM, cat. no. HY-15763), were obtained from MedChemExpress. The apoptosis inhibitor, Z-VAD-FMK (1 mM, cat. no. S7023), the necrosis inhibitor, necrostatin-1 (10 mM, cat. no. S8037), the MCT1 inhibitor, AZD3965 (10 mM, cat. no. S7339), and the glucose-6-phosphate dehydrogenase (G6PD) inhibitor, 6-aminonicotinamide (6AN, 100 mM, cat. no. S9783), were purchased form Selleck Chemicals. All reagents were dissolved in DMSO (cat. no. D2650, MilliporeSigma) for *in vitro* experiments, the treatment durations were 6 h, 12 h or 24 h, as indicated. Mice were intraperitoneally with 6AN (10 mg/kg), AZD3965 (30 mg/kg) or Fer-1 (1 mg/kg) every 2 days, respectively. All reagents were dissolved in corn oil (cat. no. C40543.36, Thermo Fisher Scientific, Inc.) for the *in vivo* experiments. H_2O_2 (5 M, cat. no. C04045101; Nanjing Chemical Reagent Co., Ltd.) were stored at 4°C and diluted with culture medium.

Healthy human serum (HHS). Healthy human blood was obtained from healthy adult donors. Donors provided written consent for using their blood, and all personal information was kept confidential as required. The experiment followed the protocol approved by the Ethics Committee of the Stomatological Hospital of Sun Yat-sen University, Guangzhou, China. The blood was centrifuged at 3,000 x g for 15 min at 4°C, and the upper serum was carefully removed and filtered through a 0.22 μm filter (MilliporeSigma) for further analysis.

Human specimen and cell culture. Chinese oral mucosal melanoma (COMM)-1 and COMM-2 cell lines were established from human mucosal melanoma specimens obtained from the Hospital of Stomatology, Sun Yat-sen University, which was followed the protocol approved by the Ethics Committee of the Stomatological Hospital of Sun Yat-sen University. The patients provided written consent for the use of their tissue in research, and all personal information was kept confidential as required. All cells were cultured in Dulbecco's modified Eagle's medium/F12 (DF12, MilliporeSigma) supplemented with 10% fetal bovine serum (FBS, Bioloical Industries). 293T cells and A375 cells were purchased from the American Type Culture Collection (ATCC) and cultured in Dulbecco's modified Eagle's medium (DMEM, MilliporeSigma) supplemented with 10% FBS (Bioloical Industries). All the cell lines were confirmed to be free of bacteria and mycoplasma contamination and cultured at 37°C in humidified chamber with 5% CO_2. All the cells treated with the different reagents including inhibitors, erastin or H_2O_2 which were cultured in serum-free DF12 supplemented with 10 μg/ml human insulin, 5 μg/ml human transferrin, 10 μg/ml heparin, 10 μg/ml ascorbic acid, 5 μg/ml bovine serum albumin-oleic acid (BSA-oleid), 10 μM 2-aminoethanol, 10 nM sodium selenite and 10 μM mercaptoethanol. The authentication of both cell lines and tissues was confirmed by short tandem repeat (STR, Guangzhou Ige Biotechnology, Ltd.).

Hematoxylin and eosin (H&E) staining, immunohistochemistry (IHC) and immunofluorescence (IF) analysis.

The primary and secondary antibodies used in the present study are presented in Table SI. The tissues were fixed in 10% formalin for 24 h, and then embedded in paraffin, and sliced into 4.5-μm-thick sections. Following deparaffinization in xylene twice for 10 min each and then rehydration in 100, 90, 80 and 70% ethanol and water for 5 min each, the sections were stained with H&E or were processed for IHC. For H&E, the sections were stained with hematoxylin (cat. no. CTS-1090; MXB Biotechnologies) at room temperature for 10 min and rinsed with tap water for 15 min. The sections were then stained with eosin and dehydrated in ascending ethanol solutions (70, 80, 90 and 100%). They were then rinsed in xylene and cover-slipped with synthetic neutral resin (cat. no. G8590-100, Beijing Solarbio Science & Technology Co., Ltd.). For IHC, the sections were incubated in fresh 3% hydrogen peroxide/methanol solution at room temperature for 10 min to quench endogenous peroxidase activity. The sections were then incubated in citrate buffer and heated at 100˚C for 10 min for antigen retrieval. After cooling, the tissue slides were washed with PBS and incubated with 5% goat serum (cat. no. AR0009; Wuhan Boster Biological Technology, Ltd.) at room temperature to block non-specific binding sites and incubated with primary antibody at 4˚C overnight. After washing with PBS, the sections were incubated with secondary antibody (cat. no. KIT-5005, MaxVision™ HRP-Polymer anti-Rabbit IHC kit; MXB Biotechnologies) at room temperature for 25 min. The sections were rinsed and stained in diaminobenzidine (DAB, cat. no. DAB-0031 MXB Biotechnologies), stained with hematoxylin at room temperature for 10 min and rinsed with tap water for 15 min. The sections were examined under a microscope (Nikon Eclipse Ni-E fluorescence microscope; Nikon Corporation).

For IF, following incubation with EdU incorporation (500 mmol, Invitrogen; Thermo Fisher Scientific, Inc.) for 2 weeks at 37˚C in humidified chamber with 5% CO_2, the cells were seeded in 24-well plates and then treated with various concentrations of sodium lactate for 48 h. Subsequently, the cells were fixed with 4% paraformaldehyde for 30 min at room temperature. After being permeabilized with 0.2% Triton X-100 in PBS for 30 min, the cells dyed with a Click-labelling dye, including 1 M CuSO4 (Wako, Japan), 1 M ascorbic acid (FUJIFILM Wako Pure Chemical Corporation), 10 μM FAM azide (Lumiprobe Corp.) for 1 h at room temperature, as previously described (46). After washing with PBS, the cells were blocked with 5% goat serum (cat. no. SP-KIT-B2, MXB Biotechnologies) at 1 h for room temperature, the cells were then stained with primary antibody at 4˚C overnight. After washing with PBS, the secondary antibody was applied for 1 h in the dark at room temperature. The samples were washed and incubated with DAPI (1:1,000; Thermo Fisher Scientific, Inc.) for 5 min, washed and mounted with fluorescence mounting medium (cat. no. S3023, Dako; Agilent Technologies, Inc.). Images were acquired using a Nikon Eclipse Ni-E fluorescence microscope. For each group, 100 pairs of cells in division were captured and the number of asymmetric division cells was calculated.

Flow cytometry (FACS) analysis. The cells (1x10^6 cells/well) were pre-seeded in 10 cm plates and the COMM-SUS cells were completely removed from the whole cell population. The COMM-AD cells were treated with PKH67 (cat. no. PKH47GL-1KT; MilliporeSigma) for 48 h according to the instructions of the manufacturer. The COMM-AD and COMM-SUS cells were then collected, and centrifuged at 140 x g for 4 min at room temperature, respectively. Stained samples were acquired using a Beckman MoFlo Astrios EQs flow cytometer (Beckman Coulter, Inc.). Data were analyzed using FlowJo V10 software (FlowJo LLC).

Animal experiments. A total of 30 female BALB/c nude mice (4-6 weeks old, weighing 16-18 g) were purchased from Guangdong Medical Laboratory Animal Center (Guangdong, China). The mice were maintained under specific pathogen-free conditions (12-h light/dark cycle, temperature of 25˚C and a relative humidity of 60%, with free access to food and water) and randomly divided into the indicated groups, including the PBS group, COMM-AD group, COMM-SUS group, COMM-AD + Fer-1 group, COMM-SUS + AZD3965 group and COMM-SUS + 6AN group (n=5/group). All the animal experiments were conducted in compliance with the National Institutes of Health Guide for the Care and Use of Laboratory Animals after approval from the Animal Ethics Committee of Sun Yat-sen University (approval no. 2020000828).

The cells with enhanced GFP (eGFP; 5x10^5 cells suspended in 100 μl PBS) were injected into the tail vein of the mice. Mice were intraperitoneally injected with 6-AN (10 mg/kg), AZD3965 (30 mg/kg) or Fer-1 (1 mg/kg) as indicated above every 2 days, respectively. After 4 weeks, the mice were anesthetized by an intraperitoneal injection of pentobarbital sodium (40 mg/kg) and euthanized by cervical dislocation. The organs were harvested and then fixed with 10% formalin for 24 h for histological analysis.

Cell viability assay. Cell viability was determined using a CellTiter-Gro® Luminescent Cell Viability Assay (cat. no. G7571; Promega Corporation). The cells were collected at the determined time points following treatment with the different reagents and seeded into a 96-well black bottom plate. An equal volume of reconstituted CellTiter-Glo reagent was added to 100 μl of cell suspension. The contents were incubated for 10 min at room temperature to stabilize the luminescent signal and cell viability was detected by record luminescence using a BioTek Synergy LX multimode reader (BioTek Instruments, Inc.). For trypan blue staining, the cells were stained with 0.4% trypan blue (cat. no. C0040; Beijing Solarbio Science & Technology Co., Ltd.) for 3 min at room temperature before counted. Unstained cells were regarded as viable, and stained cells were regarded as dead. The total cells number and the blue-positive cells number were counted using a microscope (Nikon Eclipse Ti-U; Nikon Corporation). The percentage of surviving cells was calculated using the formula: (number of total cells-number of stained cells)/number of total cells x100.

NADH, NADPH, MDA and lactate analysis. The intracellular NADH and NADPH levels were determined using a NAD+/NADH Assay kit with WST-8 (cat. no. S0175, Beyotime Institute of Biotechnology) and a NADP+/NADPH Assay kit with WST-8 (cat. no. S0179; Beyotime Institute of Biotechnology), respectively. The absorbance values were

measured at 450 nm by record luminescence using a BioTek Synergy LX multimode reader (BioTek Instruments, Inc.). The intracellular MDA expression and total protein were determined using Lipid Peroxidative MDA Assay kit (cat. no. S0131S; Beyotime Institute of Biotechnology) and a BCA Protein Assay kit (cat. no. 23227, Thermo Fisher Scientific, Inc.), respectively. MDA expression was normalized to milligram protein. Cells ($5x10^5$ cells/sample) were collected and cell lysis was performed using a Lactate Assay kit-WST (λ=450 nm, cat. no. L256; Dojindo Laboratories, Inc.). All the analyses were conducted according to the instructions of the manufacturer.

Small interfering RNA (siRNA) transfection. Synthetic siRNAs were purchased from Guangzhou RiboBio Co., Ltd. and the detailed information for the siRNAs is presented in Table SII. The transfection of the duplex siRNAs (100 nM) was carried using Lipofectamine 3000® (cat. no. L3000015; Thermo Fisher Scientific, Inc.) according to the instructions of the manufacturer. The transfection efficiency was determined at 72 h post-transfection using reverse transcription-quantitative PCR, as described below. The primer sequences used are presented in Table SIII.

Confocal microscopy. The COMM-AD cells were gently digested into single cells using 0.05% trypsin-EDTA, and the COMM-AD and COMM-SUS cells were then transferred to 35 mm confocal dishes (cat. no. FCFC020; Beyotime Institute of Biotechnology), respectively. The cells were allowed to place on glass-bottom for 5 min, and confocal imaging was performed using a Leica TCS SP8 confocal microscopy (Leica Microsystems GmbH). The light at a 405 nm wavelength was used to detect the autofluorescence of COMM-AD and COMM-SUS cells. Stacks of images were acquired using Leica LAS X software (version 2.0; Leica Microsystems GmbH), and the confocal microscope acquisition settings were kept the same for all scans.

Vectors and cell transfection. The stable overexpression of eGFP in the COMM cells was amplified from the Lenti-GFP-neo vector (Addgene, Inc.). Lentivirus were amplified from 293T packaging cells with pSPAX2 and pMD2G (Addgene, Inc.) helper plasmids. The virus-containing supernatants were collected at 48 and 72 h following transfection. The supernatants with 5% PEG8000 were centrifuged at 4,000 x g for 2 h at 4°C to concentrate the lentiviral particles, diluted in 200 μl PBS and then stored at -80°C. The COMM cells were then transfected with the lentivirus (40 μl lentivirus in 2 ml DMEM) for 8 h and then selected with 1 μg/ml puromycin (cat. no. A1113803, Gibco; Thermo Fisher Scientific, Inc.) after 48 h to stabilize eGFP expression.

RNA isolation and RT-qPCR. Total RNA was extracted using the EZ-press RNA Purification kit (cat. no. B0004DP; EZBioscience). A total of 1 μg of RNA was used for cDNA synthesis using the First Strand cDNA Synthesis kit ReverTra Ace (cat. no. FSQ-201, Toyobo Life Science) at 37°C for 10 min, 50°C for 5 min and the reaction was terminated by incubating at 95°C for 3 min. qPCR was performed using a LightCycler® 480 SYBR-Green I Master (Roche Diagnostics) according to

the manufacturer's instructions. The PCR system included 5 μl PCR mix, 0.2 μl upstream primer, 0.2 μl downstream primer, 2.6 μl RNase-free ddH$_2$O and 2 μl cDNA template. The thermocycling conditions were applied at 95°C for 5 min, followed by 45 cycles of 95°C for 10 sec, 60°C for 20 sec and then at 72°C for 20 sec. mRNA expression was normalized to hRPLP0 using the $2^{-\Delta\Delta Cq}$ method (47). The primer sequences used for RT-qPCR are presented in Table SIII.

Statistical analysis. All the experiments were carried out at least three times independently. The data are presented as the mean ± SD. Data between two groups were compared using an unpaired Student's t-test, and data among multiple groups were compared using one-way analysis of variance (ANOVA) and two-way ANOVA followed by Tukey's multiple comparisons test using GraphPad Prism Software, version 9 (GraphPad Software, Inc.). A value of P<0.05 was considered to indicate a statistically significant difference.

Results

Mucosal melanoma cells exhibit heterogeneous phenotypes. In total, two low-passage COMM cell lines, namely COMM-1 and COMM-2, were successfully established. H&E staining and melan-A immunostaining confirmed the characteristics of melanoma, whereas the COMM-1 and COMM-2 cells were verified using an STR analysis, which compared to STR profiles of primary tumor tissues (Figs. 1A and S1A and Table SIV). In addition, transmission electron microscopy (performed as described in supplementary Materials and methods; Data S1) revealed that these two low-passage cell lines were rich in melanin granules (Fig. S1B).

Compared with those of the malignant melanoma cell line, A375, cultured long-term (data not shown), the COMM-1 and COMM-2 cells exhibited highly heterogeneous phenotypes, where two potential subpopulations were identified. In particular, one exhibited a typical adherent monolayer morphology and were designated 'COMM-AD' cells (Fig. 1B). By contrast, the other sub-group proliferated in suspension and were designated as 'COMM-SUS' cells. The morphology of the COMM-AD cells was spindle-shaped, whilst that of the COMM-SUS cells exhibited a more rounded morphology (Fig. 1B).

COMM-SUS cells exhibit a greater metastatic capacity. The COMM-AD and COMM-SUS cells exhibited a dynamic conversion; the adherent cells became rounded and converted into suspension cells (Video S1). The COMM-SUS cells were completely removed from the whole cell population, following which, the COMM-AD cells were labeled with PKH67, a fluorescent reagent used for cell membrane staining, to assess the association between the COMM-AD and COMM-SUS cells (Fig. 1C). Cell viability was then assessed using trypan blue staining prior to analysis using flow cytometry. Flow cytometric analysis revealed that the majority of the COMM-SUS cells remained viable (data not shown) and were positive for PKH67 staining (Fig. 1D). A portion of COMM-AD cells transformed into COMM-SUS cells, according to the observations of template DNA co-segregation during asymmetric division (Fig. 1E). Numb immunostaining indicated that the
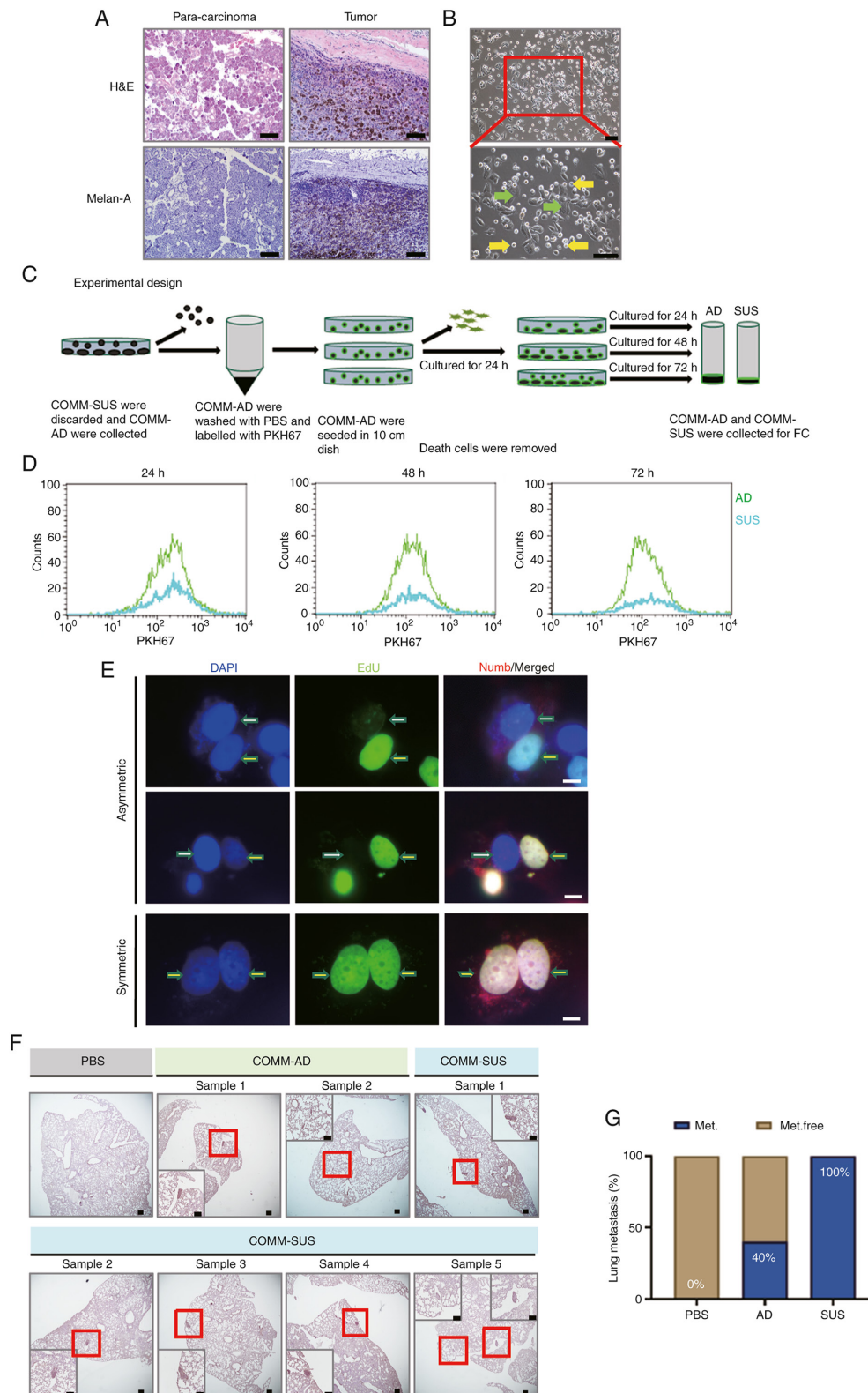
Figure 1. Malignant mucosal melanoma cells exhibited a marked heterogeneous phenotype and biological behaviors. (A) H&E and immunohistochemistry of COMM specimens. Melan-A indicated COMM cells. Scale bar, 100.0 μm. (B) Two subpopulations of COMM cells are indicated by the arrows; green arrows indicate COMM-AD cells (abbreviated as AD), and yellow arrows indicate COMM-SUS cells (abbreviated as SUS). (C) Schematic diagram of the experimental design of flow cytometric analysis. COMM-SUS cells were discarded and the whole adherent cell population was labeled with PKH67, and the cells were then seeded into culture plates for 24 h. After rinsing with the same medium, the cells were further cultured for 24, 48 and 72 h, and then analyzed by flow cytometry. (D) The results of flow cytometry of PKH67-labeled cells. (E) Immunofluorescence of template DNA co-segregate asymmetric and symmetric division. EdU (green) staining indicated distribution of DNA. Positive EdU (yellow arrows) indicated the DNA from parent cells. Negative EdU (white arrows) indicated the newly synthesized DNA. DAPI (blue) staining indicated nuclei. Numb (red) staining indicated the asymmetric division of the cell membrane. Scale bar, 10.0 μm. (F) Lung metastases were analyzed after tail intravenous injections of COMM-AD and COMM-SUS cells with eGFP, respectively at 4 weeks. Positive melan-A staining indicated COMM cells in lungs. Scale bar, 100.0 μm. (G) The frequency of developed lung metastasis in mice, expressed as a percentage (Met, metastasis-positive; Met.free, metastasis-free). n=5 mice per group. H&E, hematoxylin and eosin; COMM, Chinese oral mucosal melanoma; COMM-AD, cells with adhesive morphology; COMM-SUS, cells grown in suspension.
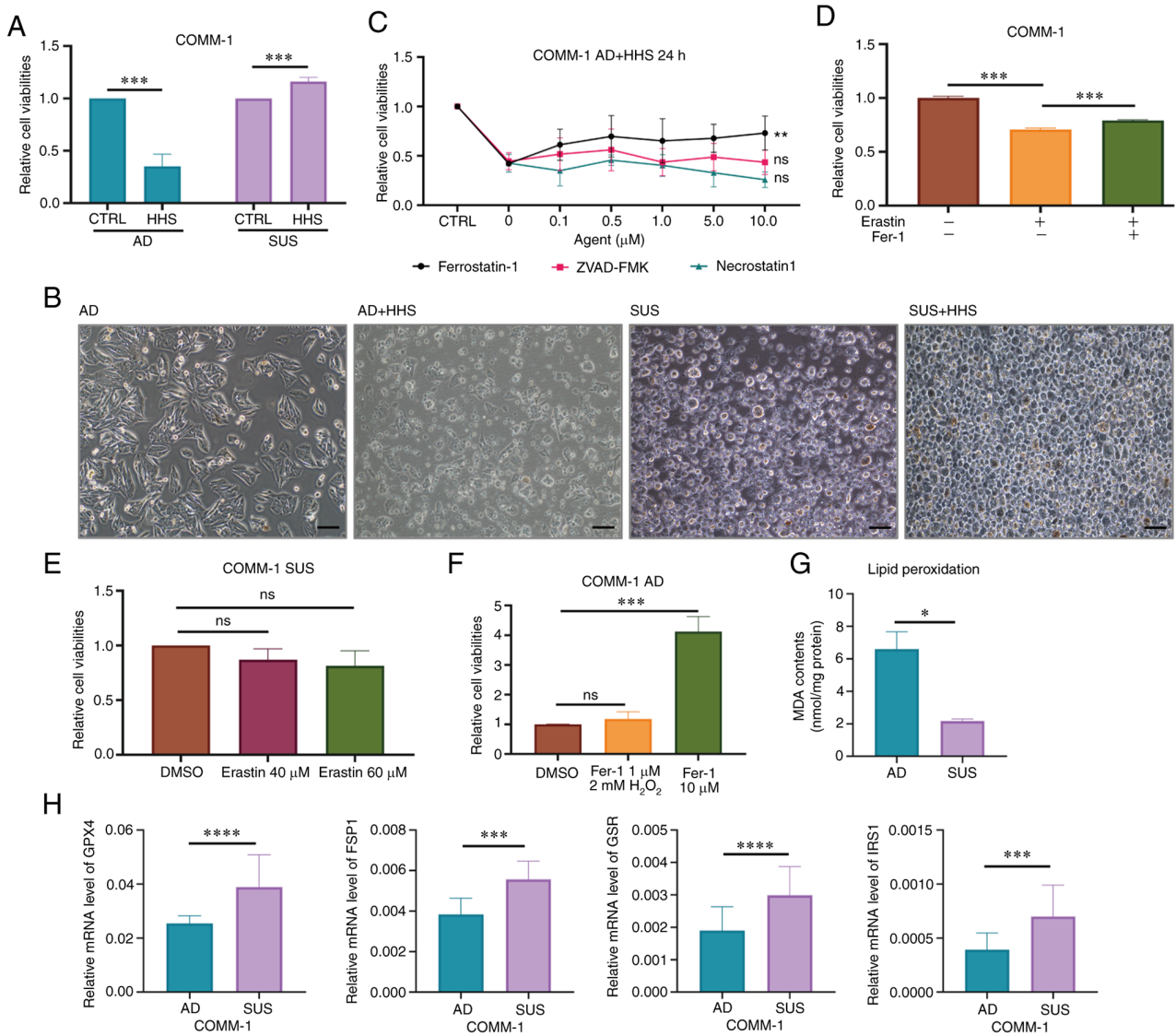
Figure 2. COMM-SUS cells survive in serum plasma by gaining an ability of anti-ferroptosis. (A) The viabilities of COMM-1 AD and COMM-1 SUS cells were measured after culturing in HHS for 24 h. (B) The cell morphology of COMM-1 AD and COMM-1 SUS cells following treatment with HHS for 24 h. (C) COMM-1 AD cells were treated with different inhibitors for 24 h. ZVAD-FMK is the inhibitor of apoptosis, ferrostatin-1 is the inhibitor of ferroptosis, and necrostatin-1 is the inhibitor of necrosis. (D) COMM-1 AD cells were treated with the ferroptosis activator, erastin, for 24 h with or without the pre-incubation of ferrostatin-1 for 6 h. (E) COMM-1 SUS cells were treated with erastin or DMSO (as the control) for 24 h. (F) COMM-1 AD cells were treated with 2 mM H2O2 for 6 h following treatment with various concentrations of ferrostatin-1 for 6 h. (G) The expression of MDA in COMM-AD and COMM-SUS cells. (H) Detection of the expression of GPX4, FSP1, GSR and IRS1 in COMM-AD and COMM-SUS cells using reverse transcription-quantitative PCR. Significance was determined using a Student's t-test or one-way ANONA or two-way ANOVA (*P<0.05, **P<0.01, ***P<0.001 and ****P<0.0001; ns, not significant, P>0.05). HHS, healthy human serum; MDA, malondialdehyde; COMM, Chinese oral mucosal melanoma; COMM-AD, cells with adhesive morphology; COMM-SUS, cells grown in suspension.

cell membrane of the COMM-AD cells was asymmetrically divided (Fig. 1E). These results suggested that the COMM-AD cells divided asymmetrically into COMM-SUS cells and maintained an interconversion state between the two subpopulations.

Equivalent quantities of eGFP-labeled COMM-AD and COMM-SUS cells (Fig. S1C) were then injected into the tail vein of immunodeficient mice to analyze their tumorigenic and metastatic potential. After 4 weeks, the mice were euthanized before immunostaining for melan-A and GFP was conducted in the lung tissues. Compared with those of the COMM-AD cells (40% metastasis), the COMM-SUS cells were more capable of establishing lesions in the lungs, with a 100% metastatic rate (Figs. 1F and G, and S1D).

COMM-SUS cells survive in blood by resisting ferroptosis. Based on the observations that the COMM-SUS cells exhibited a greater capacity for metastasis, it was hypothesized that the COMM-SUS cells resisted destruction in the blood circulation during metastasis. The COMM-AD and COMM-SUS cells were therefore cultured in HHS to evaluate their survival rates. The COMM-SUS cells appeared to be more resilient, whilst the majority of the COMM-AD cells died in HHS (Figs. 2A and B, and S2A). Subsequently, three types of cell death inhibitors were used to investigate the mechanisms underlying COMM-AD cell death in HHS. ZVAD-FMK, Fer-1 and necrostatin-1 were used to treat the COMM-AD cells. The viability of the COMM-AD cells treated with Fer-1 increased; however, ZVAD-FMK and necrostatin-1 were not

able to significantly rescue cell survival (Figs. 2C and S2B). In addition, the COMM-AD cells were treated with erastin; the majority of the COMM-AD cells died following treatment with erastin, apart from those that were pre-treated with Fer-1 (Fig. 2D). In particular, the COMM-SUS cells survived, even in the presence of erastin (Figs. 2E and S2C). Taken together, these results provided evidence of the ability of the COMM-SUS cells to resist ferroptosis. However, the COMM-AD cells presented a low metastatic capacity due to ferroptotic cell death.

Due to the critical role of ROS in the hematogenous spread of cancer cells, the capacity of resistance to oxidative stress plays a crucial anti-ferroptotic role (48). In the present study, the viability of the COMM-AD cells was found to be decreased following treatment with H_2O_2 due its potent oxidant activity, which was in turn rescued by treatment with 10 μM Fer-1 (Fig. 2F). The levels of MDA in the COMM-AD and COMM-SUS cells were then measured. The MDA content in the COMM-SUS cells was lower compared with that in the COMM-AD cells (Fig. 2G). Furthermore, RT-qPCR revealed that the COMM-SUS cells exhibited higher expression levels of GPX4, FSP1, GSR and insulin receptor substrate 1 (IRS1) compared with those in the COMM-AD cells (Figs. 2H and S2D). These observations suggested that the COMM-SUS cells survived in blood circulation by resisting ferroptosis.

Lactate metabolism is reprogrammed to promote NADH accumulation in COMM-SUS cells. Confocal microscopy images revealed a strong autofluorescence in COMM-SUS cells (Fig. 3A). Subsequent flow cytometric analysis also confirmed the high degree of autofluorescence at the 405-565 nm emission wavelengths following excitation with 405 nm (Fig. 3B). According to the range of emission wavelengths, it was suggested that the products generating this autofluorescence were NADH and NADPH (400-510 nm), lipofuscin (500-695 nm) and flavins (500-600 nm). The catalytic reactions induced by FSP1 or GPX4 are associated with the flux of NADH and NADPH. In addition, the anti-ferroptotic effects are also associated with NADH and NADPH accumulation (49,50). Considering these factors of emission wavelengths and oxidative stress resistance, it was suggested that this was caused by NADH and NADPH accumulation in COMM-SUS cells.

The intracellular NADH and NADPH levels were therefore assessed in the COMM cells. It was found that the COMM-SUS cells accumulated higher levels of NADH and NADPH (Figs. 3C and S2E). The lactate levels in the COMM-SUS cells were also found to be significantly higher compared with those in the COMM-AD cells (Figs. 3D and S2F). RT-qPCR also revealed that the COMM-SUS cells expressed MCT1 and lactate dehydrogenase (LDH)B at higher levels compared with those in the COMM-AD cells, providing a potential explanation for the higher degree of NADH accumulation observed in the COMM-SUS cells. In addition, the lower lactate flux, but higher levels of MCT4 expression in COMM-AD cells suggested that the COMM-AD cells preferentially used aerobic glycolysis, whereby lactate was transported into the extracellular space by MCT1 and MCT4, which was then consumed by COMM-SUS cells (Figs. 3E-G and S2G).

The cells were then treated with high glucose medium or glucose-free medium supplemented with various concentrations of sodium lactate according to the lactate range detected in solid tumors to test the model lactate utilization in COMM-AD and COMM-SUS cells. The intracellular lactate levels in COMM-AD cells remained relatively stable even when the concentration of exogenous sodium lactate increased. By contrast, the COMM-SUS cells exhibited a significant increase in intracellular lactate levels. Compared with the COMM-AD cells, the COMM-SUS cells took up lactate under both high glucose and glucose-free conditions (Fig. 3H). The COMM-AD and COMM-SUS cells were subsequently pre-treated with AZD3965 before being cultured in high-glucose or glucose-free medium containing various sodium lactate concentrations to assess the role of MCT1 in lactate uptake. The intracellular lactate levels were significantly increased in the COMM-AD cells treated with AZD3965 (Fig. 3H) in high-glucose medium. However, the intracellular lactate levels were decreased in the COMM-SUS cells after MCT1 was blocked (Fig. 3H). Collectively, these data suggest that the COMM-AD cells mainly utilized glucose for energy, whereas the COMM-SUS cells mainly utilized lactate as the energy source through MCT1.

A series of sodium lactate concentrations was added to the cells to examine the effects of lactate on the transformation of COMM-AD cells into COMM-SUS cells. The numbers of COMM-SUS cells were observed to be increased following treatment with increasing sodium lactate concentrations (Figs. 3I and S2H). The proportion of template DNA co-segregation during asymmetric division was also confirmed by calculating the 100 pairs of cells in division using immunofluorescence staining (Figs. 3J and S2I) in each group, suggesting that the COMM-AD cells asymmetrically divided to become lactate-accumulating COMM-SUS cells.

COMM-SUS cells are resistant to oxidative stress by accumulating NADPH through pentose phosphate pathway (PPP) activation. Although the data thus far suggested that the COMM-SUS cells principally utilized lactate as a metabolic substrate and accumulated NADH, the mechanisms underlying this phenomenon remain unknown. The classical pathways that are known to produce NADPH in cells include the PPP, fatty acid synthesis pathway (FASP) and folate metabolism pathway (FMP) (39). The key enzymes in these pathways are G6PD, 6-phosphogluconate dehydrogenase (PGD), malic enzymes (ME) 1, 2 and 3, and methylenetetrahydrofolate dehydrogenase (MTHFD)2 (Fig. 4A). RT-qPCR revealed higher expression levels of G6PD, GPD, ME2 and MTHFD2 in the COMM-SUS cells compared with those in the COMM-AD cells (Figs. 4B and S3A). However, ME1 and ME3 were not detected in either the COMM-SUS or COMM-AD cells (data not shown).

The COMM cells were subsequently transfected with siRNAs individually targeting each of the detectable enzymes to investigate which pathway was involved in NADPH production (Fig. S3B). The levels of NADH and NADPH were evaluated following the knockdown of enzyme expression. The levels of NADH and NADPH in the COMM-SUS cells were found to be significantly decreased when G6PD and PGD expression was knocked down in both the COMM-1 and
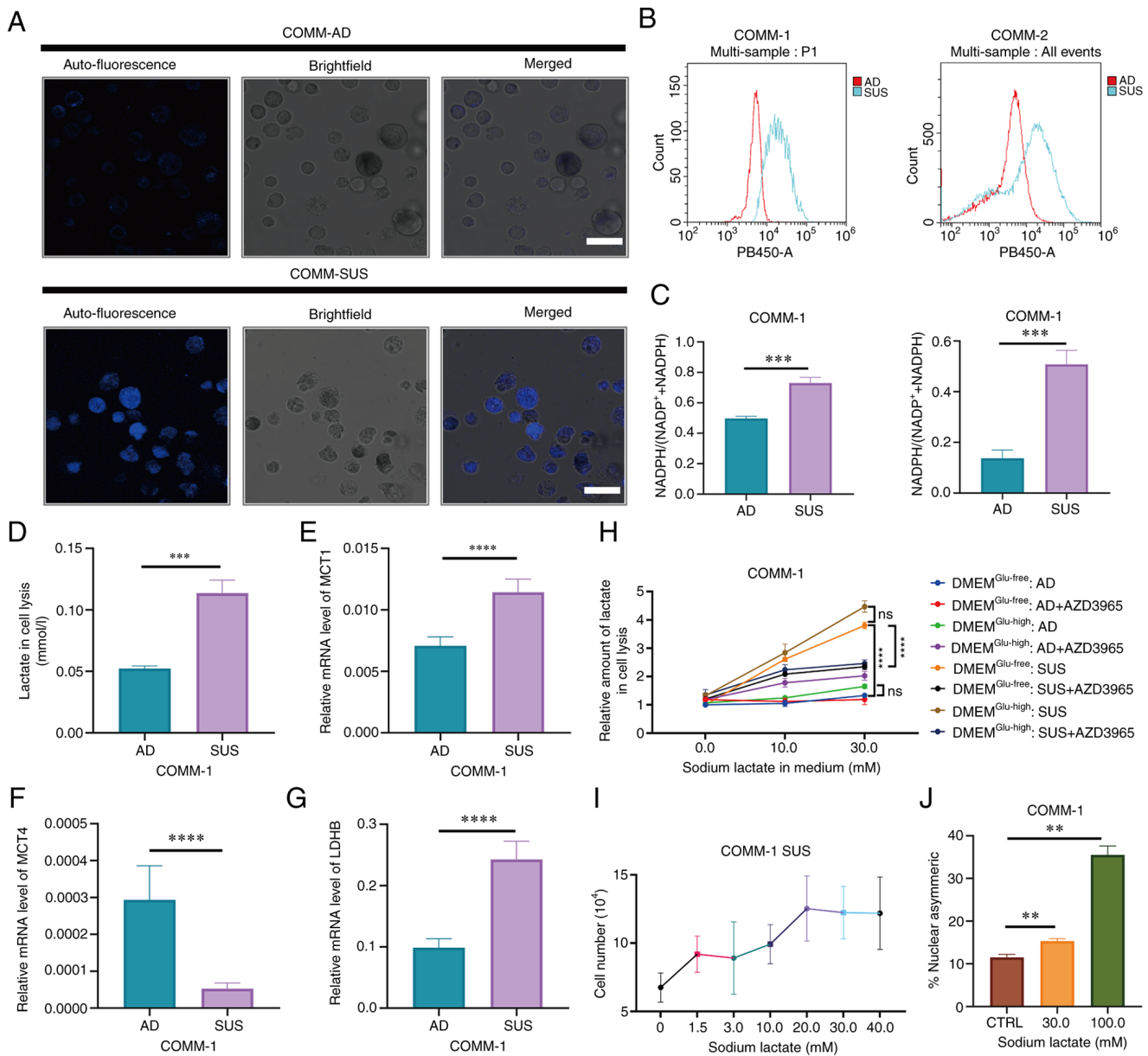
Figure 3. Lactate metabolism is reprogrammed in COMM-SUS cells. (A) Autofluorescence in COMM-AD or COMM-SUS cells was analyzed using a confocal microscope. COMM-AD cells were enzymatically digested to obtain a single-cell suspension. Scale bar, 10.0 μm. (B) Flow cytometric analysis of the autofluorescence in COMM-AD and COMM-SUS cells; the excitation wavelength was 405 nm. (C) Analyzing the amount of intracellular NADH and NADPH in COMM-1 AD and COMM-1 SUS cells. (D) The total lactate levels of COMM-1 AD and COMM-1 SUS cells were measured using a Lactate Assay kit-WST. (E-G) Reverse transcription-quantitative PCR analysis of MCT1, MCT4 and LDHB expression in COMM-1 AD and COMM-1 SUS cells. (H) COMM-1 AD and COMM-1 SUS cells were treated with or without AZD3965 for 6 h, and cultured in glucose-free medium (DMEM$^{Glu-free}$) or glucose-high medium (DMEM$^{Glu-high}$), which was supplemented with 10 and 30 mM sodium lactate for 24 h. The amount of intracellular lactate was measured. (I) The number of viable COMM-1 SUS cells was determined in 72 h after treating with a serial concentrations of sodium lactate. (J) Quantification of immunofluorescence analysis for template DNA co-segregate asymmetrically after the COMM-1 cells were treated with various concentrations of sodium lactate. Significance was determined using a Student's t-test or one-way ANONA or two-way ANOVA (**P<0.01, ***P<0.001 and ****P<0.0001; ns, not significant, P>0.05). COMM, Chinese oral mucosal melanoma; COMM-AD, cells with adhesive morphology; COMM-SUS, cells grown in suspension; MCT, monocarboxylate transporter; LDHB, lactate dehydrogenase B.

COMM-2 cell lines; however, the levels of NADH and NADPH were not altered in the COMM-AD cells (Figs. 4C and S3C). Collectively, these results suggested that the PPP was activated in the COMM-SUS cells to promote NADPH accumulation.

Lactate metabolism and PPP activation inhibit ferroptosis in COMM-SUS cells. The COMM-SUS cells were pre-treated with AZD3965 and cultured in HHS to investigate whether lactate metabolism is associated with ferroptosis. The viability

of the COMM-SUS cells was found to be significantly decreased following AZD3965 treatment (Fig. 5A). Consistent with the status in HHS, the COMM-SUS cells exhibited resistance to oxidative stress induced by H_2O_2, which was reversed by AZD3965 treatment (Fig. 5B). In addition to changes in cell viability, the intracellular NADH and NADPH levels were decreased in the COMM-SUS cells following treatment with AZD3965 (Fig. 5C and D). After MCT1 was inhibited in the COMM-AD cells, lactate was found to be accumulated in the
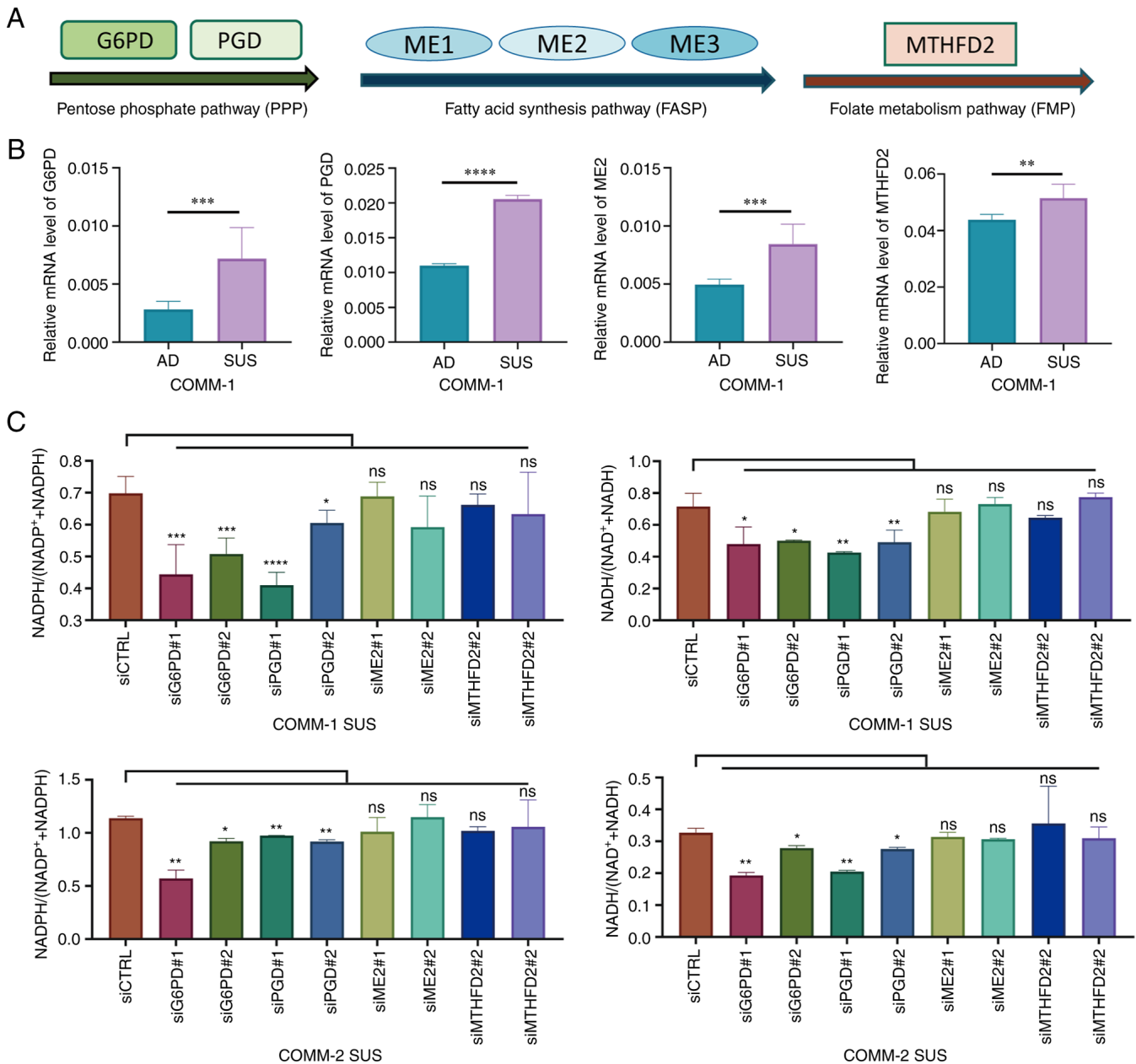
Figure 4. COMM-SUS cells resist oxidative stress by NADPH accumulation via PPP. (A) Schematic diagram of the main enzymes of the pentose phosphate pathway, fatty acid synthesis pathway and folate metabolism pathway. The expression levels of the enzymes were interfered with by corresponding siRNA. (B) The expression of the main enzymes was measured in COMM-1 AD and COMM-1 SUS cells using reverse transcription-quantitative PCR. (C) The amount of intracellular NADH and NADPH was evaluated after suppressing enzyme expression. Significance was determined using a Student's t-test or one-way ANONA (*P<0.05, **P<0.01, ***P<0.001 and ****P<0.0001; ns, not significant, P>0.05). COMM, Chinese oral mucosal melanoma; COMM-AD, cells with adhesive morphology; COMM-SUS, cells grown in suspension; PGD, 6-phosphogluconate dehydrogenase; G6PD, glucose-6-phosphate dehydrogenase.

intracytoplasmic areas, which reduced pyruvate transformation into lactate and NADH accumulation. Furthermore, the effects of lactate on the viability of COMM-AD cells were then investigated. Lactate accumulation was deleterious for the COMM-AD cells following treatment with AZD3965 to a certain extent (Figs. 5E and F, and S4A). Therefore, the COMM-AD cells were unable to resist oxidative stress after culturing in HHS even after increasing the NADH levels due to the downregulated expression of GPX4 and FSP1.

The present study validated the anti-ferroptotic efficacy of the PPP activation in COMM-SUS cells. The viability of the COMM-SUS cells was decreased following the knockdown

of associated enzymes of the three pathways separately using siRNA in HHS. Notably, cell viability was significantly decreased after PPP was inhibited by siRNA targeting G6PD and PGD enzymes (Fig. 5G and H). These results suggested that the PPP was activated in COMM-SUS cells to produce NADPH and resist serum-induced death.

Inhibition of ferroptosis increases COMM-AD cell metastasis, whilst the inhibition of MCT1 and the PPP suppresses COMM-SUS cell metastasis. The COMM-AD and COMM-SUS cells were injected into the tail vein of immunodeficient mice before Fer-1, AZD3965 and 6AN were intraperitoneally injected
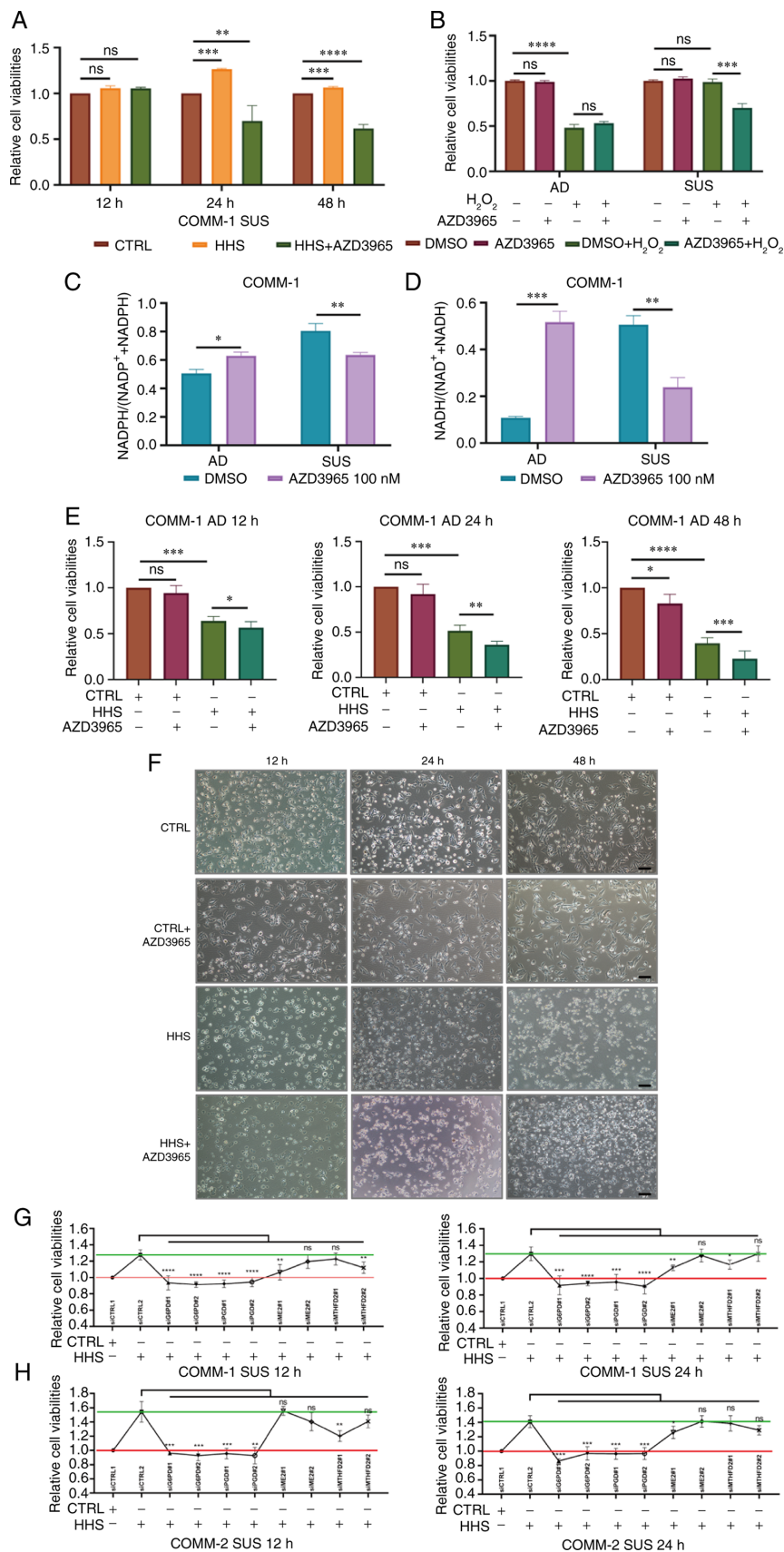
Figure 5. Lactate metabolism and pentose phosphate pathway activation inhibit ferroptosis in COMM-SUS cells. (A) COMM-1 SUS cells were treated with or without the MCT1 inhibitor, AZD3965, and then cultured in HHS for 12, 24 and 48 h. Cell viabilities were analyzed. (B) Cell viabilities of COMM-1 cells were measured following treatment with or without AZD3965 for 6 h, and cultured with 2 mM H_2O_2 for 6 h. (C and D) The amount of intracellular NADPH and NADH of COMM-1 cells were measured after treating with 100 nM AZD3965 for 24 h. (E and F) COMM-1 AD cells were treated with AZD3965, and then cultured in HHS for 12, 24 and 48 h. Cell viabilities and morphologies were analyzed. (G and H) Cell viabilities of COMM-1 SUS cells were measured after siRNA transfection targeting PPP, FASP and FMP, respectively. Significance was determined using one-way ANONA ($^*P<0.05$, $^{**}P<0.01$, $^{***}P<0.001$ and $^{****}P<0.0001$; ns, not significant, P>0.05). COMM, Chinese oral mucosal melanoma; COMM-AD, cells with adhesive morphology; COMM-SUS, cells grown in suspension; HHS, healthy human serum.
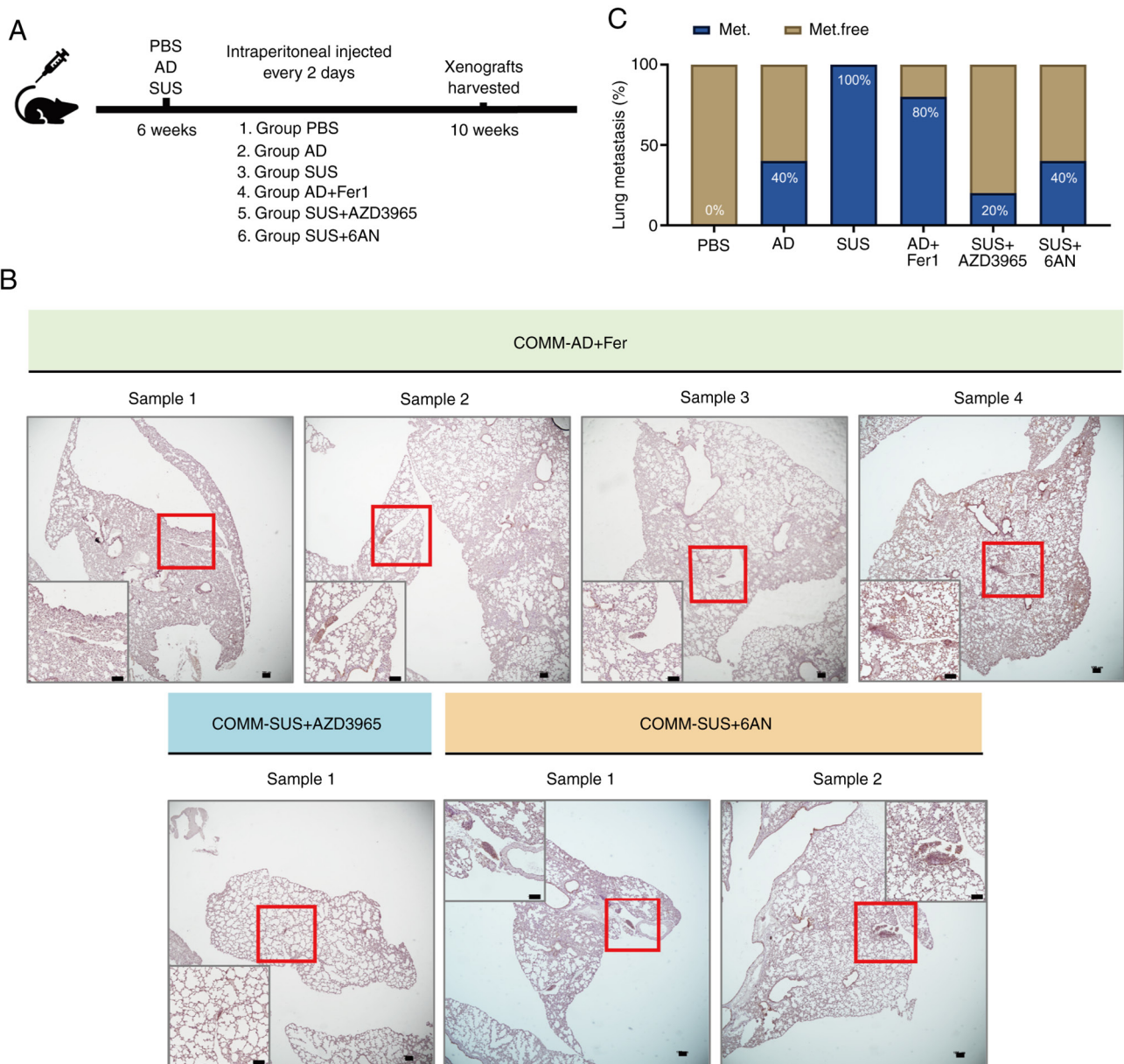
Figure 6. Inhibition of ferroptosis markedly increases the metastatic capacity of COMM-AD cells, and the inhibition of MCT1 and pentose phosphate pathway suppress the metastatic capacity of COMM-SUS cells. (A) Schematic diagram of the *in vivo* experimental design. COMM-AD and COMM-SUS cells were tail intravenously injected to 6-week old immunodeficiency mice respectively. Ferrostatin-1 (Fer-1), AZD3965 and 6AN were injected intraperitoneally every 2 days for 4 weeks in corresponding group, and the control group was injected with PBS. (B) Immunohistochemical staining of Melan-A indicated COMM cells in lung. Scale bar, 100.0 μm. (C) The frequency of developed lung metastasis of mice shown in panel B and in Fig. 1F, expressed as a percentage; n=5 mice per group. 6AN, 6-aminonicotinamide; COMM, Chinese oral mucosal melanoma; COMM-AD, cells with adhesive morphology; COMM-SUS, cells grown in suspension; MCT, monocarboxylate transporter.

every 2 days (Fig. 6A). 6AN is an anti-metabolite analog of G6PD that inhibits the NADPH-producing PPP to render the it more susceptible to oxidative stress. Consistent with the results obtained *in vitro*, 80% of the mice in the COMM-AD group treated with Fer-1 developed lung metastasis, suggesting that ferrostatin-1 improved the anti-ferroptotic capacity of the COMM-AD cells to promote metastasis. In addition, only 20% of the mice in the COMM-SUS group treated with AZD3965 and 40% of the mice in the COMM-SUS group treated with 6AN developed lung metastasis (Figs. 6B and C, and S4B). Based on these results, these observations suggest that inhibition of lactate uptake and PPP activity can significantly suppress the metastatic potential of COMM-SUS cells.

Collectively, these findings demonstrated that the COMM cells exhibited heterogenous phenotypes, where the COMM-SUS cells are able to inhibit ferroptosis and reprogram metabolism by accumulating lactate and subsequently NADH to activate the PPP, which in turn increases NADPH levels. Increased NADH and NADPH accumulation then improves the ability of COMM-SUS cells to resist oxidative stress and achieve distal metastases through hematogenous spread (Fig. 7).

Discussion

To date, cancer heterogeneity represents an ongoing challenge in clinical therapy (51). As novel technologies and reagents
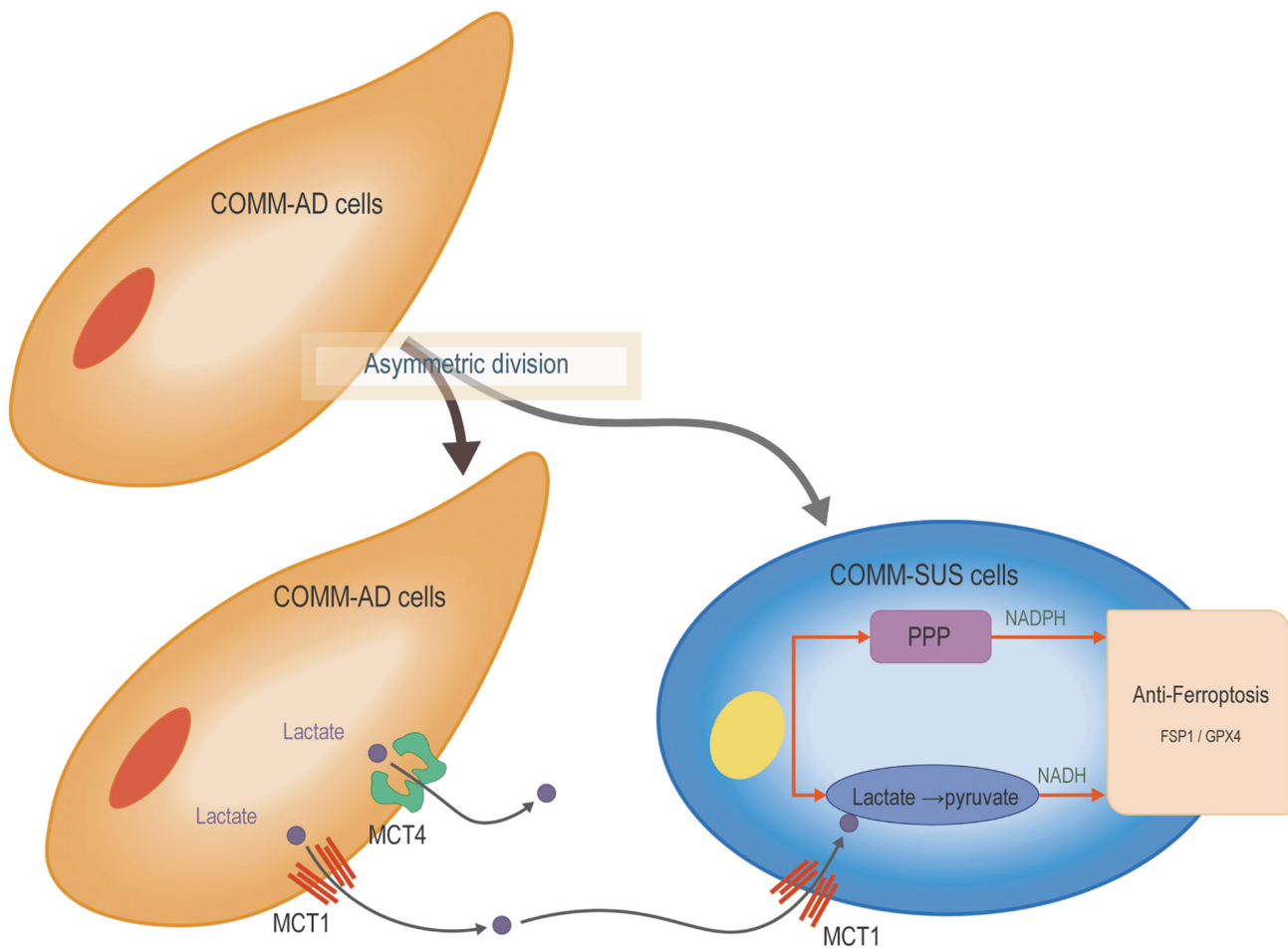
Figure 7. Metabolic heterogeneity protects metastatic mucosal melanomas from ferroptosis. COMM-AD cells asymmetrically divided into COMM-SUS cells and excreted lactate. COMM-SUS cells inhibited ferroptosis and reprogrammed metabolism by taking up more lactate to accumulate NADH and activate the PPP to increase NADPH levels. Increased NADH and NADPH accumulation improve the ability of COMM-SUS cells evade ferroptosis. COMM, Chinese oral mucosal melanoma; COMM-AD, cells with adhesive morphology; COMM-SUS, cells grown in suspension; MCT, monocarboxylate transporter; PPP, pentose phosphate pathway.

continually emerge, primary cultured cells or low-passage cell lines have been increasingly recognized for their advantages. This is due to the fact that they have been shown to retain the original heterogenous landscape, genetic and molecular profiles of their corresponding tumors (51,52). In addition, efforts have been made to characterize the biological signatures and markers of different subpopulations within the same cancer (53,54). Exploring the mechanism of tumor heterogeneity may allow for the design of strategies to interfere with the carcinogenic processes and ultimately improve cancer management in the clinic. However, the majority of cancer cell lines gradually lose their heterogeneity after long-term *in vitro* culture (43). In the present study, two MM cell lines with low-passage numbers were established to explore the heterogeneity of MM.

Cancer initiation, propagation, therapy resistance and relapse are potentially driven and maintained by asymmetric cell division (55), which also contributes to the heterogenic characteristics (56,57). In the present study, COMM-AD cells presented with template DNA co-segregation and exhibited the potential to asymmetrically divide into COMM-SUS cells, which underwent metabolic reprogramming to use lactate as their primary carbon source to enhance their own

metastatic capabilities. It has been suggested that different cell subsets within the same tumor can divide metabolic tasks by exchanging intermediary metabolites, such as lactate (58). The findings of the present study suggested that the entire COMM cell population can mimic the original tumor tissue. COMM-AD cells are cancer cells *in situ* and are considered to be glycolytic cancer cells that can produce and excrete lactate into the extracellular microenvironment (27). By contrast, the COMM-SUS cells are cancer cells that exhibit higher metastatic capacities to leave the stroma and invade by taking up lactate as the main oxidative cell type (30). This is consistent with the hypothesis of 'metabolic symbiosis' (27,30,59). Glycolytic cells use glucose to produce large quantities of lactate that are rapidly exported through MCT4, where the oxidative cells located in perfused areas use their MCT1 proteins to import the lactate (30). Once imported into the cytosol of oxidative cancer cells, lactate is then oxidized into pyruvate by LDH-1 (60). LDH typically exists as a tetramer of the LDH-H protein encoded by the *LDHB* gene and mediates the simultaneous reduction of NAD^+ into NADH (60). This pyruvate and NADH then fuel the TCA cycle to facilitate ATP production. Based on accumulating evidence, lactate is considered to be a major

carbon source for the TCA instead of being a waste product of anaerobic metabolism in cancer cells (27,61). The present study demonstrated that high levels of MCT1 expression were positively associated with metastasis and shorter overall survival times in the clinic (Fig. S4C). Based on this finding, MCT1 may represent an ideal drug target for MM treatment. The MCT1-specific inhibitor, AZD3965, has undergone a phase I clinical trial in the UK for advanced solid tumors and lymphomas (62,63). AZD3965 has been previously reported to reduce tumor growth in breast cancer (64), small cell lung cancer (63), lymphoma (65) and colon carcinoma (66). In normal proliferating cells, 30% of the intracellular NADPH has been found to be derived from the PPP, whereas the other 30% is produced from glutaminolysis flux and 40% is derived from folate metabolism (67). However, cancer cells require higher levels of NADPH for the acceleration of various physiological processes, such as biomolecule synthesis and lipid oxidation, especially redox hemostasis (68,69). Therefore, increased NADPH levels are considered to be favorable for cancer metastasis (70). Metastatic melanoma cells tend to have higher levels of NADPH generation to convert GSSG into GSH, allowing them to withstand oxidative stress through the folate pathway (14). NADPH has also been shown to promote gastric cancer growth and metastasis by upregulating the expression of ME1 (71). In the present study, in addition to lactate uptake to increase NADH levels, metabolic reprogramming in COMM-SUS cells also activated the PPP to accumulate additional NADPH levels and confer resistance to oxidative stress.

Increased NADH and NADPH accumulation not only functions as an antioxidant, but also increases autofluorescence (72,73). High levels of autofluorescence were confirmed in COMM-SUS cells in the present study. The characteristic of autofluorescence holds promise as a potentially powerful tool for detecting the first signs of metastasis during clinical diagnosis (72). Non-invasive diagnostic techniques for identifying malignant tumor cells, monitoring distant metastasis and local recurrence of cancer are improving. In particular, the use of inflammatory markers and autofluorescence to diagnose cancer holds promise (30,72,74-77). In addition, red cell distribution width (RDW) value may be applied as a novel inflammatory marker to assess malignant thyroid nodules (74). Indeed, elevated RDW values have been found in several cancer types, including esophageal cancer and gastric cancer (78-81). Tumorigenesis is frequently accompanied with alterations in the immune cell and cytokine profile (82). The degree of tumor immune infiltration altered in the tumor microenvironment, whereas the cytokine secretion profile is altered in the bloodstream (83,84). Previous studies have demonstrated that inflammation is an important hallmark of tumorigenesis, including head and neck squamous cell carcinoma and breast cancer (82,85-87). Tumors at different stages of development typically exhibit different characteristics of cancer-associated inflammation, where the different inflammatory environments will influence local immune responses (88). Therefore, the combination of inflammatory markers and autofluorescence holds diagnostic value in the clinical diagnosis of cancer.

Cancer cells are able to resist multitude of cancer therapies due to cell plasticity, which include properties of metabolic reprogramming, immune escape and suppression of cell death (56,89-91). They chronically experience high levels of oxidative stress, which may induce ferroptosis during hematogenous metastasis (92). A previous study revealed that the lymph nodes allows melanoma cells to incorporate oleic acid and other antioxidants for protection against ferroptosis (93). In the present study, notable cellular heterogeneity was observed in the mucosal MM cells tested. In particular, COMM-SUS cells exhibited highly aggressive metastatic behavior following metabolic reprogramming, resulting in the accumulation of NADH and NADPH and protection against ferroptosis induced by oxidative stress from the bloodstream. COMM-SUS cells were found to mainly depended on GPX4 and FSP1 for protection against ferroptosis. According to this finding, GPX4 or FSP1 may represent potential drug targets for suppressing MM cell metastasis. In addition, the metabolic reprogramming event that was found in the COMM-SUS cells, where increased quantities of lactate was taken up and then oxidized to pyruvate, is most likely to be associated with ferroptosis resistance. These metabolic activities resulting in or from ferroptosis are inherently associated with energy metabolism. Therefore, inhibiting metabolic reprogramming in aggressive metastatic cancer cells also represents a possible drug target to deny the high energetic needs of cancer cells.

In summary, the results from the present study suggest that efficiently metastasizing melanoma cells are able to reprogram their own metabolic pathways to increase the uptake lactate to meet their energy demands. Mechanistically, this was possibly mediated by the activation of the PPP to increase the production of the antioxidants NADH and NADPH. In addition, increases in the expression levels of GPX4 and FSP1 allowed the cells to resist ferroptotic cell death induced by oxidative stress to promote distant metastasis.

Heterogeneity is one of the important biological characteristics of cancer, which results in the existence of a diverse range of cell types and cell subpopulations with distant physiological features within the same tumor. In addition, different subpopulations of the same cancer type can utilize different synergistic mechanisms to enhance tumorigenesis. The dynamic conversion and interdependence of cancer subpopulations may provide a perspective to deepen the understanding into tumor characteristics. Cancer heterogeneity represents an ongoing challenge in clinical settings. Exploring the mechanism of cancer heterogeneity may allow research in methods of interfering with dynamic cancer inter-cell interactions and ultimately improve cancer management protocols in the clinic.

Availability of data and materials

The datasets used and/or analyzed during this study are available from the corresponding author on reasonable request.

Authors' contributions

YZ was involved in the conceptualization of the study, as well as in project administration, funding acquisition, and in the writing, reviewing and editing of the manuscript. HW was involved in the conceptualization of the study, as well as in project administration and funding acquisition. WL was involved in the conceptualization of the study, as well as in the methodology, visualization, and in the writing of the original draft. XL was involved in the conceptualization of the study, as well as in the methodology, and in the writing, reviewing and editing of the manuscript. HY was involved in the study methodology and visualization. LH, YT and SL were involved in the conceptualization of the study. WH was involved in visualization. XL and HY confirm the authenticity of all the raw data. All authors have read and approved the final manuscript.

Ethics approval and consent to participate

The specimens obtained from Hospital of Stomatology Sun Yatsen University followed the protocol approved by the Ethics Committee of the Stomatological Hospital of Sun Yat-sen University, Guangzhou, China. The patients provided written consent for the use of their blood or tissue in research. All the animal experiments were conducted in compliance with the National Institutes of Health Guide for the Care and Use of Laboratory Animals after approval from the Animal Ethics Committee of Sun Yatsen University (approval no. 2020000828).

Patient consent for publication

Not applicable.

Competing interests

The authors declare that they have no competing interests.

References

1. Spencer KR and Mehnert JM: Mucosal melanoma: Epidemiology, biology and treatment. Cancer Treat Res 167: 295-320, 2016.
2. Nassar KW and Tan AC: The mutational landscape of mucosal melanoma. Semin Cancer Biol 61: 139-148, 2020.
3. Merkel EA and Gerami P: Malignant melanoma of sun-protected sites: A review of clinical, histological, and molecular features. Lab Invest 97: 630-635, 2017.
4. Ascierto PA, Accorona R, Botti G, Farina D, Fossati P, Gatta G, Gogas H, Lombardi D, Maroldi R, Nicolai P, *et al*: Mucosal melanoma of the head and neck. Crit Rev Oncol Hematol 112: 136-152, 2017.
5. Davis LE, Shalin SC and Tackett AJ: Current state of melanoma diagnosis and treatment. Cancer Biol Ther 20: 1366-1379, 2019.
6. Yde SS, Sjoegren P, Heje M and Stolle LB: Mucosal melanoma: A literature review. Curr Oncol Rep 20: 28, 2018.
7. Poh A: First oncolytic viral therapy for melanoma. Cancer Discov 6: 6, 2016.
8. Killock D: Skin cancer: T-VEC oncolytic viral therapy shows promise in melanoma. Nat Rev Clin Oncol 12: 438, 2015.
9. Vogelstein B, Papadopoulos N, Velculescu VE, Zhou S, Diaz LA Jr and Kinzler KW: Cancer genome landscapes. Science 339: 1546-1558, 2013.
10. Chambers AF, Groom AC and MacDonald IC: Dissemination and growth of cancer cells in metastatic sites. Nat Rev Cancer 2: 563-572, 2002.
11. Suhail Y, Cain MP, Vanaja K, Kurywchak PA, Levchenko A, Kalluri R and Kshitiz: Systems biology of cancer metastasis. Cell Syst 9: 109-127, 2019.
12. Dixon SJ, Lemberg KM, Lamprecht MR, Skouta R, Zaitsev EM, Gleason CE, Patel DN, Bauer AJ, Cantley AM, Yang WS, *et al*: Ferroptosis: An iron-dependent form of nonapoptotic cell death. Cell 149: 1060-1072, 2012.
13. Mou Y, Wang J, Wu J, He D, Zhang C, Duan C and Li B: Ferroptosis, a new form of cell death: Opportunities and challenges in cancer. J Hematol Oncol 12: 34, 2019.
14. Piskounova E, Agathocleous M, Murphy MM, Hu Z, Huddlestun SE, Zhao Z, Leitch AM, Johnson TM, DeBerardinis RJ and Morrison SJ: Oxidative stress inhibits distant metastasis by human melanoma cells. Nature 527: 186-191, 2015.
15. Li D and Li Y: The interaction between ferroptosis and lipid metabolism in cancer. Signal Transduct Target Ther 5: 108, 2020.
16. Zhang Z, Lu M, Chen C, Tong X, Li Y, Yang K, Lv H, Xu J and Qin L: Holo-lactoferrin: The link between ferroptosis and radiotherapy in triple-negative breast cancer. Theranostics 11: 3167-3182, 2021.
17. Stockwell BR, Friedmann Angeli JP, Bayir H, Bush AI, Conrad M, Dixon SJ, Fulda S, Gascón S, Hatzios SK, Kagan VE, *et al*: Ferroptosis: A regulated cell death nexus linking metabolism, redox biology, and disease. Cell 171: 273-285, 2017.
18. Bersuker K, Hendricks JM, Li Z, Magtanong L, Ford B, Tang PH, Roberts MA, Tong B, Maimone TJ, Zoncu R, *et al*: The CoQ oxidoreductase FSP1 acts parallel to GPX4 to inhibit ferroptosis. Nature 575: 688-692, 2019.
19. Viswanathan VS, Ryan MJ, Dhruv HD, Gill S, Eichhoff OM, Seashore-Ludlow B, Kaffenberger SD, Eaton JK, Shimada K, Aguirre AJ, *et al*: Dependency of a therapy-resistant state of cancer cells on a lipid peroxidase pathway. Nature 547: 453-457, 2017.
20. Tsoi J, Robert L, Paraiso K, Galvan C, Sheu KM, Lay J, Wong DJL, Atefi M, Shirazi R, Wang X, *et al*: Multi-stage differentiation defines melanoma subtypes with differential vulnerability to drug-induced iron-dependent oxidative stress. Cancer Cell 33: 890-904.e5 2018.
21. Ursini F and Maiorino M: Lipid peroxidation and ferroptosis: The role of GSH and GPx4. Free Radic Biol Med 152: 175-185, 2020.
22. Faubert B, Li KY, Cai L, Hensley CT, Kim J, Zacharias LG, Yang C, Do QN, Doucette S, Burguete D, *et al*: Lactate metabolism in human lung tumors. Cell 171: 358-371.e9, 2017.
23. Hui S, Ghergurovich JM, Morscher RJ, Jang C, Teng X, Lu W, Esparza LA, Reya T, Le Zhan, Yanxiang Guo J, *et al*: Glucose feeds the TCA cycle via circulating lactate. Nature 551: 115-118, 2017.
24. Wu M, Zhang X, Zhang W, Chiou YS, Qian W, Liu X, Zhang M, Yan H, Li S, Li T, *et al*: Cancer stem cell regulated phenotypic plasticity protects metastasized cancer cells from ferroptosis. Nat Commun 13: 1371, 2022.
25. Ohshima K and Morii E: Metabolic reprogramming of cancer cells during tumor progression and metastasis. Metabolites 11: 28, 2021.
26. Icard P, Shulman S, Farhat D, Steyaert JM, Alifano M and Lincet H: How the Warburg effect supports aggressiveness and drug resistance of cancer cells? Drug Resist Updat 38: 1-11, 2018.
27. Brooks GA: The science and translation of lactate shuttle theory. Cell Metab 27: 757-785, 2018.
28. Payen VL, Mina E, Van Hée VF, Porporato PE and Sonveaux P: Monocarboxylate transporters in cancer. Mol Metab 33: 48-66, 2020.
29. Pucino V, Certo M, Bulusu V, Cucchi D, Goldmann K, Pontarini E, Haas R, Smith J, Headland SE, Blighe K, *et al*: Lactate buildup at the site of chronic inflammation promotes disease by inducing CD4+ T cell metabolic rewiring. Cell Metab 30: 1055-1074.e8, 2019.
30. Pisarsky L, Bill R, Fagiani E, Dimeloe S, Goosen RW, Hagmann J, Hess C and Christofori G: Targeting metabolic symbiosis to overcome resistance to anti-angiogenic therapy. Cell Rep 15: 1161-1174, 2016.
31. García-Cañaveras JC, Chen L and Rabinowitz JD: The tumor metabolic microenvironment: Lessons from lactate. Cancer Res 79: 3155-3162, 2019.

32. Tasdogan A, Faubert B, Ramesh V, Ubellacker JM, Shen B, Solmonson A, Murphy MM, Gu Z, Gu W, Martin M, *et al*: Metabolic heterogeneity confers differences in melanoma metastatic potential. Nature 577: 115-120, 2020.

33. Zhang G, Zhang Y, Dong D, Wang F, Ma X, Guan F and Sun L: MCT1 regulates aggressive and metabolic phenotypes in bladder cancer. J Cancer 9: 2492-2501, 2018.

34. Felmlee MA, Jones RS, Rodriguez-Cruz V, Follman KE and Morris ME: Monocarboxylate transporters (SLC16): Function, regulation, and role in health and disease. Pharmacol Rev 72: 466-485, 2020.

35. Rabinowitz JD and Enerbäck S: Lactate: The ugly duckling of energy metabolism. Nat Metab 2: 566-571, 2020.

36. Gao HJ, Zhao MC, Zhang YJ, Zhou DS, Xu L, Li GB, Chen MS and Liu J: Monocarboxylate transporter 4 predicts poor prognosis in hepatocellular carcinoma and is associated with cell proliferation and migration. J Cancer Res Clin Oncol 141: 1151-1162, 2015.

37. Wang Y, Li Y, Jiang L, Ren X, Cheng B and Xia J: Prognostic value of glycolysis markers in head and neck squamous cell carcinoma: A meta-analysis. Aging (Albany NY) 13: 7284-7299, 2021.

38. Pertega-Gomes N, Felisbino S, Massie CE, Vizcaino JR, Coelho R, Sandi C, Simoes-Sousa S, Jurmeister S, Ramos-Montoya A, Asim M, *et al*: A glycolytic phenotype is associated with prostate cancer progression and aggressiveness: A role for monocarboxylate transporters as metabolic targets for therapy. J Pathol 236: 517-530, 2015.

39. Wilde L, Roche M, Domingo-Vidal M, Tanson K, Philp N, Curry J and Martinez-Outschoorn U: Metabolic coupling and the reverse Warburg effect in cancer: Implications for novel biomarker and anticancer agent development. Semin Oncol 44: 198-203, 2017.

40. Huhta H, Helminen O, Palomäki S, Kauppila JH, Saarnio J, Lehenkari PP and Karttunen TJ: Intratumoral lactate metabolism in Barrett's esophagus and adenocarcinoma. Oncotarget 8: 22894, 2017.

41. Hu Y and Zeng F: Expressions of GPR81, MCT1 and MCT4 in squamous carcinoma and their clinical significance. Zhong Nan Da Xue Xue Bao Yi Xue Ban 43: 950-956, 2018 (In Chinese).

42. Nakayama Y, Torigoe T, Inoue Y, Minagawa N, Izumi H, Kohno K and Yamaguchi K: Prognostic significance of monocarboxylate transporter 4 expression in patients with colorectal cancer. Exp Ther Med 3: 25-30, 2012.

43. Hubert CG, Rivera M, Spangler LC, Wu Q, Mack SC, Prager BC, Couce M, McLendon RE, Sloan AE and Rich JN: A three-dimensional organoid culture system derived from human glioblastomas recapitulates the hypoxic gradients and cancer stem cell heterogeneity of tumors found in vivo. Cancer Res 76: 2465-2477, 2016.

44. Post Y, Puschhof J, Beumer J, Kerkkamp HM, de Bakker MA, Slagboom J, de Barbanson B, Wevers NR, Spijkers XM, Olivier T, *et al*: Snake venom gland organoids. Cell 180: 233-247. e21, 2020.

45. Boretto M, Maenhoudt N, Luo X, Hennes A, Boeckx B, Bui B, Heremans R, Perneel L, Kobayashi H, Van Zundert I, *et al*: Patient-derived organoids from endometrial disease capture clinical heterogeneity and are amenable to drug screening. Nat Cell Biol 21: 1041-1051, 2019.

46. Haider N, Dutt P, van de Kooij B, Ho J, Palomero L, Pujana MA, Yaffe M and Stambolic V: NEK10 tyrosine phosphorylates p53 and controls its transcriptional activity. Oncogene 39: 5252-5266, 2020.

47. Livak KJ and Schmittgen TD: Analysis of relative gene expression data using real-time quantitative PCR and the 2(-Delta Delta C(T)) method. Methods 25: 402-408, 2001.

48. Park E and Chung SW: ROS-mediated autophagy increases intracellular iron levels and ferroptosis by ferritin and transferrin receptor regulation. Cell Death Dis 10: 822, 2019.

49. Ding CC, Rose J, Sun T, Wu J, Chen PH, Lin CC, Yang WH, Chen KY, Lee H, Xu E, *et al*: MESH1 is a cytosolic NADPH phosphatase that regulates ferroptosis. Nat Metab 2: 270-277, 2020.

50. Zheng J and Conrad M: The metabolic underpinnings of ferroptosis. Cell Metab 32: 920-937, 2020.

51. Dagogo-Jack I and Shaw AT: Tumour heterogeneity and resistance to cancer therapies. Nat Rev Clin Oncol 15: 81-94, 2018.

52. Burrell RA, McGranahan N, Bartek J and Swanton C: The causes and consequences of genetic heterogeneity in cancer evolution. Nature 501: 338-345, 2013.

53. Zheng H, Pomyen Y, Hernandez MO, Li C, Livak F, Tang W, Dang H, Greten TF, Davis JL, Zhao Y, *et al*: Single-cell analysis reveals cancer stem cell heterogeneity in hepatocellular carcinoma. Hepatology 68: 127-140, 2018.

54. Wang DC and Wang X: Systems heterogeneity: An integrative way to understand cancer heterogeneity. Semin Cell Dev Biol 64: 1-4, 2017.

55. Hitomi M, Chumakova AP, Silver DJ, Knudsen AM, Pontius WD, Murphy S, Anand N, Kristensen BW and Lathia JD: Asymmetric cell division promotes therapeutic resistance in glioblastoma stem cells. JCI Insight 6: e130510, 2021.

56. Marjanovic ND, Weinberg RA and Chaffer CL: Cell plasticity and heterogeneity in cancer. Clin Chem 59: 168-179, 2013.

57. Gerlach C, Rohr JC, Perié L, van Rooij N, van Heijst JW, Velds A, Urbanus J, Naik SH, Jacobs H, Beltman JB, *et al*: Heterogeneous differentiation patterns of individual CD8^{+} T cells. Science 340: 635-639, 2013.

58. Bergers G and Fendt SM: The metabolism of cancer cells during metastasis. Nat Rev Cancer 21: 162-180, 2021.

59. Yu L, Chen X, Wang L and Chen S: The sweet trap in tumors: Aerobic glycolysis and potential targets for therapy. Oncotarget 7: 38908-38926, 2016.

60. Brisson L, Bański P, Sboarina M, Dethier C, Danhier P, Fontenille MJ, Van Hée VF, Vazeille T, Tardy M, Falces J, *et al*: Lactate dehydrogenase B controls lysosome activity and autophagy in cancer. Cancer Cell 30: 418-431, 2016.

61. Kennedy KM, Scarbrough PM, Ribeiro A, Richardson R, Yuan H, Sonveaux P, Landon CD, Chi JT, Pizzo S, Schroeder T and Dewhirst MW: Catabolism of exogenous lactate reveals it as a legitimate metabolic substrate in breast cancer. PLoS One 8: e75154, 2013.

62. Silva A, Antunes B, Batista A, Pinto-Ribeiro F, Baltazar F and Afonso J: In vivo anticancer activity of AZD3965: A systematic review. Molecules 27: 181, 2021.

63. Polański R, Hodgkinson CL, Fusi A, Nonaka D, Priest L, Kelly P, Trapani F, Bishop PW, White A, Critchlow SE, *et al*: Activity of the monocarboxylate transporter 1 inhibitor AZD3965 in small cell lung cancer. Clin Cancer Res 20: 926-937, 2014.

64. Benyahia Z, Blackman MC, Hamelin L, Zampieri LX, Capeloa T, Bedin ML, Vazeille T, Schakman O and Sonveaux P: In vitro and in vivo characterization of MCT1 inhibitor AZD3965 confirms preclinical safety compatible with breast cancer treatment. Cancers (Basel) 13: 569, 2021.

65. Beloueche-Babari M, Wantuch S, Casals Galobart T, Koniordou M, Parkes HG, Arunan V, Chung YL, Eykyn TR, Smith PD and Leach MO: MCT1 inhibitor AZD3965 increases mitochondrial metabolism, facilitating combination therapy and noninvasive magnetic resonance spectroscopy. Cancer Res 77: 5913-5924, 2017.

66. Wang G, Wang JJ, Yin PH, Xu K, Wang YZ, Shi F, Gao J and Fu XL: New strategies for targeting glucose metabolism-mediated acidosis for colorectal cancer therapy. J Cell Physiol 234: 348-368, 2018.

67. Fan J, Ye J, Kamphorst JJ, Shlomi T, Thompson CB and Rabinowitz JD: Quantitative flux analysis reveals folate-dependent NADPH production. Nature 510: 298-302, 2014.

68. Pavlova NN and Thompson CB: The emerging hallmarks of cancer metabolism. Cell Metab 23: 27-47, 2016.

69. Lewis CA, Parker SJ, Fiske BP, McCloskey D, Gui DY, Green CR, Vokes NI, Feist AM, Vander Heiden MG and Metallo CM: Tracing compartmentalized NADPH metabolism in the cytosol and mitochondria of mammalian cells. Mol Cell 55: 253-263, 2014.

70. Wang X, Liu Z, Sun J, Song X, Bian M, Wang F, Yan F and Yu Z: Inhibition of NADPH oxidase 4 attenuates lymphangiogenesis and tumor metastasis in breast cancer. FASEB J 35: e21531, 2021.

71. Lu YX, Ju HQ, Liu ZX, Chen DL, Wang Y, Zhao Q, Wu QN, Zeng ZL, Qiu HB, Hu PS, *et al*: ME1 regulates NADPH homeostasis to promote gastric cancer growth and metastasis. Cancer Res 78: 1972-1985, 2018.

72. Tamošiūnas M, Plorina EV, Lange M, Derjabo A, Kuzmina I, Bļiznuks D and Spigulis J: Autofluorescence imaging for recurrence detection in skin cancer postoperative scars. J Biophotonics 13: e201900162, 2020.

73. Huang TT, Chen KC, Wong TY, Chen CY, Chen WC, Chen YC, Chang MH, Wu DY, Huang TY, Nioka S, *et al*: Two-channel autofluorescence analysis for oral cancer. J Biomed Opt 24: 1-10, 2018.

74. Gulali A, Mustafa S, Ibrahim K, Erkus E, Ozer B, Kocak MZ, Yaman S, Keyif F, Altinordu R, Erkol H and Savli H: Could red cell distribution width be a marker of thyroid cancer? J Coll Physicians Surg Pak 27: 556-558, 2017.

75. Chamma E, Qiu J, Lindvere-Teene L, Blackmore KM, Majeed S, Weersink R, Dickie CI, Griffin AM, Wunder JS, Ferguson PC and DaCosta RS: Optically-tracked handheld fluorescence imaging platform for monitoring skin response in the management of soft tissue sarcoma. J Biomed Opt 20: 076011, 2015.

76. Waaijer L, Filipe MD, Simons J, van der Pol CC, de Boorder T, van Diest PJ and Witkamp AJ: Detection of breast cancer precursor lesions by autofluorescence ductoscopy. Breast Cancer 28: 119-129, 2021.

77. Borile G, Sandrin D, Filippi A, Anderson KI and Romanato F: Label-free multiphoton microscopy: Much more than fancy images. Int J Mol Sci 22: 2657, 2021.

78. Salvagno GL, Sanchis-Gomar F, Picanza A and Lippi G: Red blood cell distribution width: A simple parameter with multiple clinical applications. Crit Rev Clin Lab Sci 52: 86-105, 2015.

79. Ma W, Mao S, Bao M, Wu Y, Guo Y, Liu J, Wang R, Li C, Zhang J, Zhang W and Yao X: Prognostic significance of red cell distribution width in bladder cancer. Transl Androl Urol 9: 295-302, 2020.

80. Wang PF, Song SY, Guo H, Wang TJ, Liu N and Yan CX: Prognostic role of pretreatment red blood cell distribution width in patients with cancer: A meta-analysis of 49 studies. J Cancer 10: 4305, 2019.

81. Han F, Liu Y, Cheng S, Sun Z, Sheng C, Sun X, Shang X, Tian W, Wang X, Li J, *et al*: Diagnosis and survival values of neutrophil-lymphocyte ratio (NLR) and red blood cell distribution width (RDW) in esophageal cancer. Clin Chim Acta 488: 150-158, 2019.

82. Ghosh M, Saha S, Bettke J, Nagar R, Parrales A, Iwakuma T, van der Velden AWM and Martinez LA: Mutant p53 suppresses innate immune signaling to promote tumorigenesis. Cancer Cell 39: 494-508.e5, 2021.

83. Watson MJ, Vignali PDA, Mullett SJ, Overacre-Delgoffe AE, Peralta RM, Grebinoski S, Menk AV, Rittenhouse NL, DePeaux K, Whetstone RD, *et al*: Metabolic support of tumour-infiltrating regulatory T cells by lactic acid. Nature 591: 645-651, 2021.

84. Karsten E, Breen E, McCracken SA, Clarke S and Herbert BR: Red blood cells exposed to cancer cells in culture have altered cytokine profiles and immune function. Sci Rep 10: 7727, 2020.

85. Li ZX, Zheng ZQ, Wei ZH, Zhang LL, Li F, Lin L, Liu RQ, Huang XD, Lv JW, Chen FP, *et al*: Comprehensive characterization of the alternative splicing landscape in head and neck squamous cell carcinoma reveals novel events associated with tumorigenesis and the immune microenvironment. Theranostics 9: 7648-7665, 2019.

86. Diakos CI, Charles KA, McMillan DC and Clarke SJ: Cancer-related inflammation and treatment effectiveness. Lancet Oncol 15: e493-e503, 2014.

87. Duan Q, Zhang H, Zheng J and Zhang L: Turning cold into hot: Firing up the tumor microenvironment. Trends Cancer 6: 605-618, 2020.

88. Hou J, Karin M and Sun B: Targeting cancer-promoting inflammation-have anti-inflammatory therapies come of age? Nat Rev Clin Oncol 18: 261-279, 2021.

89. Yu Y, Yan Y, Niu F, Wang Y, Chen X, Su G, Liu Y, Zhao X, Qian L, Liu P and Xiong Y: Ferroptosis: A cell death connecting oxidative stress, inflammation and cardiovascular diseases. Cell Death Discov 7: 193, 2021.

90. Meacham CE and Morrison SJ: Tumour heterogeneity and cancer cell plasticity. Nature 501: 328-337, 2013.

91. Boumahdi S and de Sauvage FJ: The great escape: Tumour cell plasticity in resistance to targeted therapy. Nat Rev Drug Discov 19: 39-56, 2020.

92. Zhou B, Zhang JY, Liu XS, Chen HZ, Ai YL, Cheng K, Sun RY, Zhou D, Han J and Wu Q: Tom20 senses iron-activated ROS signaling to promote melanoma cell pyroptosis. Cell Res 28: 1171-1185, 2018.

93. Ubellacker JM, Tasdogan A, Ramesh V, Shen B, Mitchell EC, Martin-Sandoval MS, Gu Z, McCormick ML, Durham AB, Spitz DR, *et al*: Lymph protects metastasizing melanoma cells from ferroptosis. Nature 585: 113-118, 2020.